

# FlowCritic: Bridging Value Estimation with Flow Matching in Reinforcement Learning

Shan Zhong, Shutong Ding, He Diao, Xiangyu Wang, Kah Chan Teh, and Bei Peng\*



**Abstract**—Reliable value estimation serves as the cornerstone of reinforcement learning (RL) by evaluating long-term returns and guiding policy improvement, significantly influencing the convergence speed and final performance. Existing works improve the reliability of value function estimation via multi-critic ensembles and distributional RL, yet the former merely combines multi point estimation without capturing distributional information, whereas the latter relies on discretization or quantile regression, limiting the expressiveness of complex value distributions. Inspired by flow matching’s success in generative modeling, we propose a generative paradigm for value estimation, named FlowCritic. Departing from conventional regression for deterministic value prediction, FlowCritic leverages flow matching to model value distributions and generate samples for value estimation. Specifically, FlowCritic formulates the target value distribution through distributional Bellman operators, and trains a velocity field network to learn the continuous probability flow from a tractable prior distribution to the target distribution, thereby enabling flexible modeling of arbitrarily complex value distributions. More importantly, FlowCritic introduces the coefficient of variation (CoV) of the generated value distribution to quantify the noise level of training samples. Based on CoV, FlowCritic adaptively weights samples to prioritize those with low noise, thereby reducing the variance of policy gradient during backpropagation. Additionally, FlowCritic incorporates truncated sampling and velocity field clipping mechanisms to ensure training stability. Our theoretical analysis demonstrates FlowCritic’s convergence and advantages. Extensive experiments on 12 IsaacGym benchmarks demonstrate FlowCritic’s superiority over existing RL baselines, while its successful deployment on a real quadrupedal robot platform validates its effectiveness in practical physical systems. Notably, FlowCritic is the first approach to integrate flow matching into value distribution modeling for RL, and offers a new perspective on the effective exploitation of distributional information.

**Code:** [https://github.com/smartXiaoz/kalman\\_flowc.git](https://github.com/smartXiaoz/kalman_flowc.git)<sup>1</sup>.

**Index Terms**—Reinforcement Learning, Value Estimation, Flow Matching, Generative Modeling

*This work was supported by NSFC, China (51975107), and in part by the China Scholarship Council under Grant CSC202406070141. Corresponding author: Bei Peng.*

*S. Zhong, He Diao, Xiangyu Wang, and B. Peng are with the School of Mechanical and Electrical Engineering, University of Electronic Science and Technology of China, Chengdu 611731, China (e-mail: 202211040927@std.uestc.edu.cn; 202311040616@std.uestc.edu.cn; 202322040551@std.uestc.edu.cn; beipeng@uestc.edu.cn);. Bei Peng is also with Sichuan EIR Technology Co. Ltd.*

*S. Ding is with the School of Information Science and Technology, ShanghaiTech University. (dingsht@shanghaitech.edu.cn)*

*K. C. Teh is with the School of Electrical and Electronic Engineering, Nanyang Technological University, Singapore. (e-mail: ekcteh@ntu.edu.sg).*

<sup>1</sup> The repository is currently private and will be made public upon publication.

## 1 INTRODUCTION

Reinforcement Learning (RL) has achieved remarkable success in recent years and has been widely applied to numerous challenging domains, such as robotic control [1]–[5], autonomous driving [6], [7], and post-training of large language models [8], [9]. The value function lies at the core of RL, as it directly determines the algorithm’s ability to efficiently evaluate the long-term returns of states or actions, thereby dictating its convergence speed and final performance [10]–[12]. However, value estimation faces the dual challenges of bias and high variance, stemming from the inherent stochasticity of the environment, exploration noise in the policy, and the intrinsic errors of function approximation [13]–[17].

To enhance the robustness of value estimation, researchers have conducted numerous valuable explorations. For instance, generalized advantage estimation (GAE) [17] flexibly balances the bias-variance trade-off by using an exponentially-weighted sum of temporal difference (TD) errors, while methods such as Double Q-learning [18] and Twin Delayed Deep Deterministic policy gradient algorithm (TD3) [19] mitigate the overestimation problem through decoupling or taking the minimum of value estimates. Furthermore, ensembles of independent value networks have been leveraged to improve robustness. Specifically, averaged-DQN reduces variance by averaging over a history of value networks [20]. Maxmin Q-learning [21] and Soft Actor-Critic-N (SAC-N) [22] suppress overestimation bias by maintaining multiple value functions and selecting the minimum estimate. The multi-critic architecture similarly stabilizes the training process by averaging several value estimates [23].

An alternative perspective is offered by Distributional Reinforcement Learning (DRL), whose core idea is to learn the full probability distribution of the value function, rather than merely estimating its expectation [24], [25]. The pioneering work Categorical 51 (C51) discretizes the support of the Q-value into a fixed set of atoms and learns a categorical distribution [24]. Subsequently, quantile Regression Deep Q-Network (QR-DQN) learns discrete quantiles of the distribution via quantile regression [26], while Implicit Quantile Networks (IQN) maps a base probability to its corresponding Q-value using an implicit quantile network [27], which enables more precise yet still discrete modeling of the value distribution. Further developments include Distributional

Soft Actor-Critic (DSAC), which adopts a Gaussian assumption for value distributions within the SAC framework [28], [29], and Truncated Quantile Critics (TQC), which employs an ensemble of quantile critics to enhance the stability of value distribution modeling [30].

The aforementioned methods have improved value estimation robustness from different perspectives. Nevertheless, advancing RL performance via improved value functions faces two key problems:

- 1) Discrete Approximation of Value Function: Both multi-critic ensembles and DRL fundamentally rely on regression-based approximation to learn deterministic value mappings [10], [31]. Each network in an ensemble produces a fixed point estimate, with the ensemble merely aggregating these finite outputs. While DRL extends value functions to distributional representations, the methods that rely on Gaussian assumptions or quantile discretization inherently constrain the distribution family, thereby limiting the flexibility to capture complex value distributions [25].
- 2) Unexploited Value Distribution Statistics: Existing methods typically extract only the mean or a conservative estimate from value distributions for policy guidance, which neglects higher-order statistical features of the value distribution [30], [32]. These statistical features may characterize the stochasticity of interactions with the environment and the noise level during exploration for each learning sample, yet they are not fully exploited in RL, which limits the potential for policy optimization.

Inspired by the recent success of flow matching in generative modeling [33]–[36], we propose a general framework for value distribution modeling, named FlowCritic, which represents the value function as a samplable generative model. Compared to conventional regression-based methods, FlowCritic leverages the expressive power of flow matching to approximate arbitrarily complex value distribution, and exploits generative sampling to effectively extract distributional statistics to guide RL training. Specifically, FlowCritic formulates target value distribution using distributional Bellman operators. Subsequently, a velocity field network is trained to match the instantaneous velocity that transports the prior Gaussian distribution to the target distribution, which is then integrated via an ordinary differential equation (ODE) to generate the value estimates. Further, truncated sampling and velocity field clipping are introduced to enhance training robustness. Truncated sampling discards extreme high values to reduce outlier effects, while velocity field clipping limits the magnitude of velocity field updates to stabilize the flow matching model’s convergence.

Moreover, inspired by signal processing principles, we re-examine the exploitation of distributional information. A key insight is that return estimates across states have varying reliability. For instance, the value network produces more reliable estimates for trained samples than for unseen ones, and environment stochasticity further affect estimate quality, where we use noise levels to characterize the quality differences across different state estimates. However, existing algorithms treat all training samples equally and ignore the noise levels of value estimates, which causes

high-noise samples to propagate excessive variance during gradient backpropagation, degrading training stability and hindering convergence. Accordingly, FlowCritic introduces the coefficient of variation (CoV), a second-order statistic of the value distribution, to quantify noise levels across training samples, where CoV is derived from multiple value estimates generated via ODE integration. Low-CoV samples provide more reliable value estimates than high-CoV samples. Accordingly, FlowCritic assigns higher weights to low-CoV samples and lower weights to high-CoV ones through adaptive weighting, enabling reliable value estimates to guide policy optimization, thereby reducing variance of policy gradients and enhancing sample efficiency in RL training. Our contributions are summarized as follows:

- 1) We are the first to introduce flow matching into RL value modeling, proposing a generative paradigm for modeling arbitrarily complex value distributions. Furthermore, we provide theoretical convergence analysis for this approach.
- 2) FlowCritic innovatively exploits the CoV from value distributions to weight training samples adaptively, thereby reducing gradient variance. We also provide theoretical analysis of this weighting advantage. Additionally, truncated sampling and velocity field clipping mechanisms ensure training robustness.
- 3) Extensive experiments on twelve IsaacGym benchmarks demonstrate that our instantiation of FlowCritic significantly outperforms baselines. Its successful deployment on a real quadrupedal robot further validates practical effectiveness in physical systems.

The remainder of this paper is organized as follows. We begin by introducing the necessary background in Section 2. Section 3 presents an example of the proposed FlowCritic paradigm to illustrate its implementation, followed by a theoretical analysis in Section 4. We then present extensive experimental results to validate our approach in Section 5. Finally, Section 6 concludes the paper and discusses future work.

## 2 PRELIMINARIES

### 2.1 Online Reinforcement Learning

RL problems are typically formulated as a Markov Decision Process (MDP) [37], represented by a 5-tuple  $(\mathcal{S}, \mathcal{A}, P, r, \gamma)$ , where  $\mathcal{S}$  and  $\mathcal{A}$  denote the state and action spaces respectively,  $P(s_{t+1}|s_t, a_t)$  is the transition probability,  $r_t = r(s_t, a_t)$  is the immediate reward, and  $\gamma \in [0, 1]$  is the discount factor. An agent interacts with the environment through a parameterized policy  $\pi_\theta(a_t|s_t)$ , generating trajectories  $\tau = (s_0, a_0, r_0, s_1, \dots)$ , with the objective of maximizing the expected cumulative discounted return:  $J(\pi_\theta) = \mathbb{E}_{\tau \sim \pi_\theta} [\sum_{t=0}^{\infty} \gamma^t r_t]$ . To achieve this objective, RL algorithms rely on value functions to evaluate and improve policies. Value functions can be categorized into two main types: the state value function  $V^\pi(s) = \mathbb{E}_\pi [\sum_{t=0}^{\infty} \gamma^t r_t | s_0 = s]$ , which estimates the expected return from a given state, and the action value function  $Q^\pi(s, a) = \mathbb{E}_\pi [\sum_{t=0}^{\infty} \gamma^t r_t | s_0 = s, a_0 = a]$ , which estimates the expected return after taking a specific action. These value functions form the foundation for different algorithmic paradigms.

Value-based methods primarily rely on action value functions for decision-making. For instance, methods like DQN learn  $Q_\phi(s, a)$  to directly select optimal actions by minimizing TD errors [18], [20]:

$$\mathcal{L}_Q = \mathbb{E} \left[ \left( Q_\phi(s_t, a_t) - \left( r_t + \gamma \max_{a'} Q_{\phi'}(s_{t+1}, a') \right) \right)^2 \right]. \quad (1)$$

In contrast, policy gradient methods utilize state value functions to evaluate policy performance through advantage estimation. The advantage function  $A^\pi(s, a) = Q^\pi(s, a) - V^\pi(s)$  measures how much better an action is compared to the average, commonly computed via GAE [17]:

$$\hat{A}_t = \sum_{l=0}^{T-t-1} (\gamma \lambda)^l \delta_{t+l}, \quad \delta_t = r_t + \gamma V_\phi(s_{t+1}) - V_\phi(s_t), \quad (2)$$

where  $\lambda \in [0, 1]$  controls the bias-variance trade-off. The empirical return target is constructed as:

$$\hat{R}_t = \sum_{l=0}^{T-t-1} (\gamma \lambda)^l \delta_{t+l} + V_\phi(s_t). \quad (3)$$

The state value function  $V_\phi(s)$  is then trained to fit this target by minimizing the mean squared error:

$$\mathcal{L}_V = \mathbb{E}_t \left[ \left( V_\phi(s_t) - \hat{R}_t \right)^2 \right]. \quad (4)$$

It is evident that both Q-function and V-function are approximated through regression networks producing deterministic point estimates, which deprives them of the potential to exploit value distributional statistics for policy learning.

## 2.2 Flow Matching Methods

Flow matching is an emerging generative modeling method. It learns a time-dependent velocity field to establish continuous transport between a prior distribution and the target distribution [35], [36], [38]. Let the data distribution be  $p_{\text{data}}(x)$  and the prior distribution be  $p_{\text{prior}}(\varepsilon)$ . A time-dependent interpolation path is defined as:

$$o^t = tx + (1-t)\varepsilon, \quad x \sim p_{\text{data}}, \quad \varepsilon \sim p_{\text{prior}}, \quad (5)$$

where the conditional velocity at time  $t$  is given by

$$u^t(o^t | x) = \frac{do^t}{dt} = x - \varepsilon. \quad (6)$$

Since the same  $o^t$  may be generated from different pairs  $(x, \varepsilon)$ , the conditional velocity  $u^t(o^t | x)$  is not unique. To capture the averaged dynamics over all possible paths, flow matching introduces the concept of marginal velocity, which at time  $t$  is defined as:

$$u(o^t, t) = \mathbb{E}_{p(u^t | o^t)} [u^t(o^t | x)], \quad (7)$$

where  $p(u^t | o^t)$  denotes the conditional distribution of velocities given a fixed  $o^t$ . During training, the objective is to make the neural network  $f_\theta(o^t, t)$  approximate the true marginal velocity  $u(o^t, t)$ . The corresponding loss function is formulated as:

$$\mathcal{L}_{\text{FM}}(\theta) = \mathbb{E}_{t, p_t(o^t)} [\|f_\theta(o^t, t) - u^t(o^t, x)\|^2], \quad (8)$$

However, the exact marginal velocity  $u(o^t, t)$  in Eq. (8) is intractable, as it requires computing a conditional expectation over all possible  $(x, \varepsilon)$  pairs given  $o^t$ . To overcome this issue, conditional flow matching (CFM) replaces the marginal velocity field with the conditional velocity field  $u^t(o^t | x)$  and proves their equivalence in expectation [35]. The training objective of CFM is therefore expressed as:

$$\mathcal{L}_{\text{CFM}}(\theta) = \mathbb{E}_{t, x \sim p_{\text{data}}, \varepsilon \sim p_{\text{prior}}} [\|f_\theta(o^t, t) - u^t(o^t | x)\|^2]. \quad (9)$$

Once trained, the flow matching model can leverage an ODE solver to efficiently generate data by integrating along the learned velocity field, starting from the prior distribution. In this work, we adopt  $\varepsilon \sim \mathcal{N}(0, 1)$  as the prior.

**Notation:** To avoid ambiguity, we distinguish between two types of timesteps: the subscript  $t$  denotes the environment timestep in RL, e.g.,  $s_t$  indicates the state at timestep  $t$ ; the superscript  $t$  denotes the continuous interpolation time in flow matching, e.g.,  $o^t$  represents the variable along the flow at interpolation time  $t \in [0, 1]$ .

## 3 METHODS

This section presents the implementation of the FlowCritic paradigm. Specifically, we instantiate it within the policy gradient framework using PPO as the base algorithm [39], given its proven stability, scalability, and extensive adoption in robotics and complex control tasks. It is important to emphasize that FlowCritic is a general paradigm and can be readily integrated with various RL methods.

### 3.1 Value Distribution Modeling via Flow Matching

We extend the conventional expectation form  $V^\pi(s) = \mathbb{E}_\pi[\sum_{t=0}^{\infty} \gamma^t r_t | s_0 = s]$  to a distributional perspective by defining the random return

$$Z^\pi(s) \triangleq \sum_{t=0}^{\infty} \gamma^t r_t, \quad Z^\pi(s) \sim p^\pi(\cdot | s), \quad (10)$$

where  $Z^\pi(s)$  is the random variable of discounted cumulative returns. This naturally induces the distributional Bellman expectation operator  $\mathcal{T}^\pi$ , which maps any conditional distribution  $p \in \mathcal{M}$  to

$$(\mathcal{T}^\pi p)(\cdot | s) \triangleq r(s, a) + \gamma Z(s'), \quad (11)$$

with  $Z(s') \sim p(\cdot | s')$ .

Hence, we construct a parameterized distribution  $p_\theta^\pi(\cdot | s)$  based on the flow matching to approximate the true return distribution  $p^\pi(\cdot | s)$ . Unlike standard applications of flow matching that train on readily available datasets, it is infeasible to draw samples directly from the true return distribution  $p^\pi(\cdot | s)$  in RL. Naively adopting this scalar  $\hat{R}_t$  as the training target would fundamentally contradict our objective of modeling the return distribution, as it would constrain the flow matching model to approximate merely the expected return  $\mathbb{E}[Z^\pi(s)]$  rather than capturing the  $p^\pi(\cdot | s)$ . To resolve this conflict, FlowCritic introduces a distributional bootstrapping mechanism, which commences with the definition of the distributional TD sample:

$$\zeta_t = r_t + \gamma \mathcal{F}_\theta(s_{t+1}, \varepsilon_{t+1}) - \mathcal{F}_\theta(s_t, \varepsilon_t), \quad (12)$$

where  $\mathcal{F}_\theta(s, \varepsilon)$  represents the mapping that transforms a sample  $\varepsilon$  from the prior distribution into a return sample  $z^1 \sim p_\theta^\pi(\cdot | s)$ . While the prior distribution can be arbitrary, we use the standard Gaussian distribution  $\varepsilon \sim \mathcal{N}(0, 1)$  in this work. This transformation is achieved by solving the following ODE from  $t = 0$  to  $t = 1$ :

$$\frac{d\mathbf{o}^t}{dt} = f_\theta(\mathbf{o}^t, t, s), \quad \text{with initial condition } \mathbf{o}^0 = \varepsilon. \quad (13)$$

The resulting sample is thus given by

$$z^1 := \mathbf{o}^1 = \mathcal{F}_\theta(s, \varepsilon) \sim p_\theta^\pi(\cdot | s). \quad (14)$$

In this paper, we approximate this solution using the Euler method with 5 iterations, where each step uses a fixed integration step size  $\Delta t$  as follows:

$$\mathbf{o}^{t+\Delta t} = \mathbf{o}^t + \Delta t \cdot f_\theta(\mathbf{o}^t, t, s). \quad (15)$$

Building upon this distributional TD sample, the final distributional return target  $\hat{z}_t$  is constructed as follows:

$$\hat{z}_t = \sum_{l=0}^{T-t-1} (\gamma \lambda)^l \zeta_{t+l} + \mathcal{F}_\theta(s_t, \varepsilon_t). \quad (16)$$

Subsequently, a linear interpolation path  $\mathbf{o}^t$  is then constructed to connect the prior sample to the target return:

$$\mathbf{o}^t = (1-t)\varepsilon + t\hat{z}_t, \quad t \in [0, 1], \quad (17)$$

where  $t$  parameterizes the interpolation. The instantaneous velocity field along this path is given by

$$u^t(\mathbf{o}^t | \hat{z}_t) = \frac{d\mathbf{o}^t}{dt} = \hat{z}_t - \varepsilon. \quad (18)$$

We incorporate the state  $s$  as an explicit condition into the velocity prediction network  $f_\theta(\mathbf{o}^t, t, s)$ , thereby implementing a classifier-free guidance mechanism. The training objective is defined as:

$$\mathcal{L}_{\text{CFM}}(\theta) = \mathbb{E}_{s, \varepsilon, z, \hat{z}_t, t} \left[ \left\| f_\theta(\mathbf{o}^t, t, s) - u^t(\mathbf{o}^t | \hat{z}_t) \right\|^2 \right]. \quad (19)$$

The minimization of (19) optimizes the network  $f_\theta$  to model the velocity field that maps the prior distribution to the state-value distribution. This paradigm of directly learning a continuous transformation marks a fundamental departure from prior approximation methods, such as C51 and QR-DQN, that rely on discrete support points. Consequently, this approach endows FlowCritic with a superior expressive capacity, enabling it to capture arbitrary return distributions.

### 3.2 Robust Value Learning with Truncation and Clipping

To ensure stable learning of the value distribution during bootstrapping, we introduce a clipping mechanism for the velocity field updates. This method constrains the change between the current velocity field network  $f_\theta$ , and a target network  $f_{\theta_{\text{old}}}$ . For a given state  $s_t$ , interpolation point  $\mathbf{o}^t$ , and time  $t$ , their respective predictions are:

$$v_t^{\text{new}} = f_\theta(s_t, \mathbf{o}^t, t), \quad v_t^{\text{old}} = f_{\theta_{\text{old}}}(s_t, \mathbf{o}^t, t). \quad (20)$$

The clipping mechanism then constrains the deviation of the new prediction from the old one to construct a regularized velocity  $v_t^{\text{clipped}}$ :

$$v_t^{\text{clipped}} = v_t^{\text{old}} + \text{clip}(v_t^{\text{new}} - v_t^{\text{old}}, -\delta, \delta), \quad (21)$$

where the threshold  $\delta > 0$  controls the maximum allowable update size, thereby preventing disruptive changes to the learned velocity field. Finally, the flow matching loss (19) can be rewritten with the clipping mechanism as

$$\mathcal{L}_{\text{CFM}}(\theta) = \mathbb{E}_{s, \varepsilon, z, t} \left[ \max \left( \|v_t^{\text{new}} - \hat{u}^t\|^2, \|v_t^{\text{clipped}} - \hat{u}^t\|^2 \right) \right]. \quad (22)$$

The policy improvement phase requires a stable estimate of the advantage function  $\hat{A}_t$  to ensure a reliable update direction. To obtain a low-variance value baseline, we estimate the conditional expectation  $V(s) = \mathbb{E}[Z^\pi(s)]$  via Monte Carlo sampling. For a given state  $s_t$ , we draw  $n$  independent samples  $\{\varepsilon_i\}_{i=1}^n \sim \mathcal{N}(0, 1)$  from the prior distribution and transform them through the learned flow to generate  $n$  return estimates:

$$z_{t,i} = \mathcal{F}_\theta(s_t, \varepsilon_i), \quad i = 1, \dots, n, \quad (23)$$

where  $z_{t,i}$  denotes the  $i$ -th return sample generated for state  $s_t$ . The empirical mean of these samples provides the value estimate:

$$\hat{V}(s_t) = \frac{1}{n} \sum_{i=1}^n z_{t,i}. \quad (24)$$

To counteract the overestimation bias caused by high-return samples generated by the flow model, we use a truncated estimator that discards the top  $m$  of  $n$  sorted samples  $(z_{t,[i]})$ , the truncated estimator is defined as:

$$\hat{V}_{\text{trunc}}(s_t) = \frac{1}{n-m} \sum_{i=1}^{n-m} z_{t,[i]}. \quad (25)$$

Then, we compute the TD errors using  $\hat{V}_{\text{trunc}}(s)$  as the baseline:

$$\delta_t = r_t + \gamma \hat{V}_{\text{trunc}}(s_{t+1}) - \hat{V}_{\text{trunc}}(s_t). \quad (26)$$

The advantage estimate  $\hat{A}_t$  is then computed via GAE by aggregating these TD errors with exponential weighting:

$$\hat{A}_t = \sum_{l=0}^{T-t-1} (\gamma \lambda)^l \delta_{t+l}. \quad (27)$$

In FlowCritic, truncation and clipping work in a concerted effort to enhance training stability and robustness. Truncation mitigates the estimation bias from extreme high-return samples, and provides a natural form of pessimism early in optimization. Meanwhile, clipping constrains excessive updates when the deviation between new and old predictions grows too large, ensuring a stable learning process.

### 3.3 Weighted Policy Optimization via Value Distribution Modeling

To fully exploit the structural information within the value distribution, we adopt a signal processing perspective, where we treat the set of return samples  $\{z_{t,i}\}_{i=1}^n$  as a collection of noisy observations of the true value  $V^*(s_t)$ . A critical property of these observations is that their noise level is not constant; instead, it varies significantly across different states as a direct consequence of the environment's intrinsic stochasticity and the uncertainty inherent in trajectory sampling. Consequently, uniformly treating samples with

**Algorithm 1:** FlowCritic

---

1 **Require:** Discount factor  $\gamma$ ; GAE parameter  $\lambda$ ; PPO clipping coefficient  $\epsilon$ ; velocity field clipping threshold  $\delta$ ; CoV temperature  $\alpha$ ; number of samples  $n$ ; truncation size  $m$ ; number of parallel environments  $N_e$ ; rollout length  $T$ ; number of epochs  $K$ ; minibatch size  $B$

2 Initialize policy parameters  $\theta_\pi$  and flow matching model parameters  $\theta_f$ ;

3 **for**  $iteration = 1, 2, \dots$  **do**

4   Collect trajectories by interacting with  $N_e$  parallel environments for  $T$  steps to obtain dataset  $\mathcal{D} = \{(s_t^{(i)}, a_t^{(i)}, r_t^{(i)}, s_{t+1}^{(i)})\}$  (Eq. (28));

5   **for** each state  $s_t$  in  $\mathcal{D}$  **do**

6     Construct distributional return target  $\hat{z}_t$  (Eq. (16));

7     Sample  $\{\varepsilon_i\}_{i=1}^n \sim \mathcal{N}(0, 1)$  from the prior distribution;

8     Generate return samples  $\{z_{t,i}\} = \{\mathcal{F}_{\theta_f}(s_t, \varepsilon_i)\}_{i=1}^n$  via flow matching;

9     Compute truncated value estimate  $\hat{V}(s_t)$  (Eq. (25));

10    Calculate advantage (Eq. (27));

11    Compute state-dependent weight  $w_t$  based on CoV (Eq. (31));

12   **end**

13   **for** epoch  $k = 1, \dots, K$  **do**

14     Shuffle dataset  $\mathcal{D}$  and split into minibatches of size  $B$ ;

15     **for** each minibatch  $\mathcal{B} \subset \mathcal{D}$  **do**

16       Update flow matching model: minimize clipped flow matching loss (Eq. (22));

17        $\theta_f \leftarrow \theta_f - \eta_f \nabla_{\theta_f} \mathcal{L}_{\text{CFM}}(\theta_f; \mathcal{B})$ ;

18       Update policy: maximize weighted PPO objective (Eq. (32));

19        $\theta_\pi \leftarrow \theta_\pi + \eta_\pi \nabla_{\theta_\pi} \mathcal{L}_{\text{WPPO}}(\theta_\pi; \mathcal{B})$ ;

20     **end**

21   **end**

22 **end**

---

varying Signal-to-Noise Ratios (SNRs) is suboptimal, as this approach allows high-noise samples to introduce excessive variance into the policy gradient, thereby degrading the algorithm's performance. Therefore, we propose an adaptive weighting mechanism for policy optimization, as illustrated in Fig. 1.

Specifically, we generate rollouts by executing the current policy  $\pi_\theta$  for  $T$  timesteps across  $N_e$  parallel environments. These trajectories are gathered into a temporary collection  $\mathcal{D}$ :

$$\mathcal{D} = \{(s_t^{(k)}, a_t^{(k)}, r_t^{(k)}, s_{t+1}^{(k)}) \mid t = 0, \dots, T-1, k = 1, \dots, N_e\}, \quad (28)$$

where  $k$  indexes the parallel environments,  $s_t^{(k)}$  denotes the state at step  $t$  in the  $k$ -th environment, and  $|\mathcal{D}| = N_e \times T$ . For each state  $s_t^{(k)}$  in  $\mathcal{D}$ , we then generate a set of  $n$  return samples by applying the sampling operation defined in Eq. (23). This yields the following sample set for each

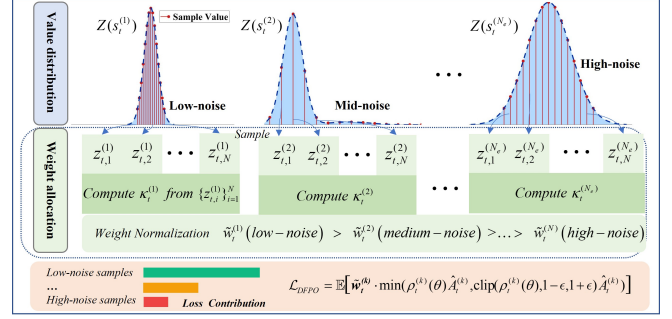


Fig. 1. FlowCritic weighting mechanism. Value distributions with lower noise levels receive larger weights in policy optimization, ensuring that reliable estimates dominate the learning process.

state:

$$\{z_{t,i}^{(k)}\}_{i=1}^n = \{\mathcal{F}_{\theta_f}(s_t, \varepsilon_i)\}_{i=1}^n, \quad (29)$$

where  $z_{t,i}^{(k)}$  denotes the  $i$ -th generated return for state  $s_t^{(k)}$ .

To adaptively quantify the noise level, we introduce the CoV, denoted by  $\kappa_t^{(k)}$ :

$$\kappa_t^{(k)} = \frac{\sigma_t^{(k)}}{|\mu_t^{(k)}| + \varepsilon}, \quad \varepsilon = 10^{-8}, \quad (30)$$

where  $\mu_t^{(k)} = \frac{1}{n} \sum_{i=1}^n z_{t,i}^{(k)}$  is the mean of the return samples for state  $s_t^{(k)}$ , and  $\sigma_t^{(k)} = \sqrt{\frac{1}{n} \sum_{i=1}^n (z_{t,i}^{(k)} - \mu_t^{(k)})^2}$  is their standard deviation. In contrast to directly using the standard deviation, the CoV accounts for the magnitude of returns when measuring noise, thereby avoiding weight biases arising from differences in absolute value scales and enabling an adaptive balancing of sample importance across states.

Based on  $\kappa_t^{(k)}$ , the state-level sample weight is defined as:

$$w_t^{(k)} = \exp(-\alpha \cdot \kappa_t^{(k)}), \quad (31)$$

where  $\alpha > 0$  is a hyperparameter. In practice, these weights are normalized across the batch:  $\tilde{w}_t^{(k)} = \frac{w_t^{(k)}}{\sum_{j,l} w_l^{(j)}} \cdot N_e \cdot T$  to ensure  $\sum_{k,t} \tilde{w}_t^{(k)} = N_e \cdot T$ . Finally, incorporating these normalized weights into the PPO objective yields the weighted loss function:

$$\mathcal{L}_{\text{FlowCritic}}(\theta) = \mathbb{E}_{(s_t^{(k)}, a_t^{(k)}) \sim \mathcal{D}} \left[ \tilde{w}_t^{(k)} \cdot \min \left( \rho_t^{(k)}(\theta) \hat{A}_t^{(k)}, \right. \right. \left. \left. \text{clip}(\rho_t^{(k)}(\theta), 1-\epsilon, 1+\epsilon) \hat{A}_t^{(k)} \right) \right], \quad (32)$$

where  $\rho_t^{(k)}(\theta) = \frac{\pi_\theta(a_t^{(k)} | s_t^{(k)})}{\pi_{\theta_{\text{old}}}(a_t^{(k)} | s_t^{(k)})}$  is the importance sampling ratio, the advantage function  $\hat{A}_t^{(k)}$  is computed according to Eq. (27). The weight term  $\tilde{w}_t^{(k)}$  in  $\mathcal{L}_{\text{WPPO}}$  thus functions as an adaptive filter, explicitly suppressing the influence of high-noise samples on gradient estimation while amplifying high-confidence observations, thereby enhancing both the stability and convergence efficiency of policy updates.

Based on the above formulations, the complete training procedure of FlowCritic is summarized in Algorithm 1.

## 4 THEORETICAL ANALYSIS

To further elucidate the properties of FlowCritic, we analyze its convergence from a theoretical perspective, it can be shown that the distributional approximation process of FlowCritic is convergent, while the velocity field clipping mechanism provides additional stability during training. Before proceeding, we provide the following definitions and lemmas.

**Definition 1.** Let  $\mu, \nu \in \mathcal{P}_p(\mathbb{R})$ , where  $\mathcal{P}_p(\mathbb{R})$  denotes the set of probability measures on  $\mathbb{R}$  with finite  $p$ -th moment ( $p \geq 1$ ). The  $p$ -Wasserstein distance between  $\mu$  and  $\nu$  is defined as

$$W_p(\mu, \nu) = \left( \inf_{\pi \in \Pi(\mu, \nu)} \mathbb{E}_{(X, Y) \sim \pi} [|X - Y|^p] \right)^{1/p}, \quad (33)$$

where  $\Pi(\mu, \nu)$  denotes the set of all couplings of  $\mu$  and  $\nu$ . For two conditional distributions  $p, q \in \mathcal{M}$ , we define the supremum metric as

$$\bar{W}_p(p, q) = \sup_{s \in \mathcal{S}} W_p(p(\cdot | s), q(\cdot | s)). \quad (34)$$

**Definition 2.** Let  $\{p_{\theta_k}^\pi\}_{k=0}^\infty \subset \mathcal{M}$  denote the sequence of conditional return distributions generated by FlowCritic during training. The approximation error at iteration  $k + 1$  is defined as

$$\varepsilon_{k+1} = \bar{W}_p\left(p_{\theta_{k+1}}^\pi, \mathcal{T}^\pi p_{\theta_k}^\pi\right), \quad (35)$$

where  $\mathcal{T}^\pi$  denotes the distributional Bellman expectation operator as defined in Eq. (11).

**Lemma 1.** If  $X' = X + c$  and  $Y' = Y + c$  with corresponding distributions  $\mu'$  and  $\nu'$ , then

$$W_p(\mu', \nu') = W_p(\mu, \nu). \quad (36)$$

**Lemma 2.** If  $X' = aX$  and  $Y' = aY$  with corresponding distributions  $\mu'$  and  $\nu'$ , then

$$W_p(\mu', \nu') = |a| W_p(\mu, \nu). \quad (37)$$

**Lemma 3.** For any  $\mu, \nu, \lambda \in \mathcal{P}_p(\mathbb{R})$ , it holds that

$$W_p(\mu, \lambda) \leq W_p(\mu, \nu) + W_p(\nu, \lambda). \quad (38)$$

Furthermore, for any  $p, q, r \in \mathcal{M}$ , we have

$$\bar{W}_p(p, r) \leq \bar{W}_p(p, q) + \bar{W}_p(q, r). \quad (39)$$

**Theorem 1** (Convergence of Approximate Value Distribution Iteration). *If the single-step approximation errors of FlowCritic satisfy  $\varepsilon_{t+1} \leq \varepsilon_{\max}$  for all  $t \geq 0$ , then the sequence of value distributions  $\{p_{\theta_t}^\pi\}$  converges to a neighborhood of the true value distribution  $p^\pi$ :*

$$\limsup_{t \rightarrow \infty} \bar{W}_p(p_{\theta_t}^\pi, p^\pi) \leq \frac{\varepsilon_{\max}}{1 - \gamma}.$$

*Proof.* Let  $p_\theta^\pi, p_{\theta'}^\pi \in \mathcal{M}$  be two approximate value distributions generated by FlowCritic. By equation (11),  $(\mathcal{T}^\pi p_\theta^\pi)(\cdot | s)$  and  $(\mathcal{T}^\pi p_{\theta'}^\pi)(\cdot | s)$  represent the distributions of  $r(s, a) + \gamma Z_\theta(s')$  and  $r(s, a) + \gamma Z_{\theta'}(s')$  respectively, where  $a \sim \pi(\cdot | s)$ ,  $s' \sim P(\cdot | s, a)$ ,  $Z_\theta(s') \sim p_\theta^\pi(\cdot | s')$ , and  $Z_{\theta'}(s') \sim p_{\theta'}^\pi(\cdot | s')$ .

We denote  $P_{s, \pi}(a, s') = \pi(a | s)P(s' | s, a)$  as the joint distribution of  $(a, s')$  given  $s$ . For each fixed  $(a, s')$ , let

$\mu_{s, a, s'}^{(\theta)}$  and  $\mu_{s, a, s'}^{(\theta')}$  be the conditional distributions of  $r(s, a) + \gamma Z_\theta(s')$  and  $r(s, a) + \gamma Z_{\theta'}(s')$  respectively. We then have:

$$(\mathcal{T}^\pi p_\theta^\pi)(\cdot | s) = \int_{(a, s')} \mu_{s, a, s'}^{(\theta)} dP_{s, \pi}(a, s'), \quad (40)$$

$$(\mathcal{T}^\pi p_{\theta'}^\pi)(\cdot | s) = \int_{(a, s')} \mu_{s, a, s'}^{(\theta')} dP_{s, \pi}(a, s'). \quad (41)$$

For a fixed  $s \in \mathcal{S}$ , let  $\Pi_s$  denote all couplings  $\xi$  with marginals  $(\mathcal{T}^\pi p_\theta^\pi)(\cdot | s)$  and  $(\mathcal{T}^\pi p_{\theta'}^\pi)(\cdot | s)$ . Similarly, for each  $(a, s')$ , let  $\Pi_{a, s'}$  denote all couplings  $\xi_{a, s'}$  with marginals  $\mu_{s, a, s'}^{(\theta)}$  and  $\mu_{s, a, s'}^{(\theta')}$ . Based on the coupling formulation of Wasserstein distance, we obtain:

$$W_p^p((\mathcal{T}^\pi p_\theta^\pi)(\cdot | s), (\mathcal{T}^\pi p_{\theta'}^\pi)(\cdot | s)) = \inf_{\xi \in \Pi_s} \int \int |x - y|^p d\xi(x, y). \quad (42)$$

Similarly, we have::

$$W_p^p(\mu_{s, a, s'}^{(\theta)}, \mu_{s, a, s'}^{(\theta')}) = \inf_{\xi_{a, s'} \in \Pi_{a, s'}} \int \int |x - y|^p d\xi_{a, s'}(x, y). \quad (43)$$

Let  $\xi_{a, s'}^*$  be the optimal coupling achieving the infimum in (43). Since both mixtures share the same mixing measure  $P_{s, \pi}$ , we construct the coupling:

$$\hat{\xi} = \int_{(a, s')} \xi_{a, s'}^* dP_{s, \pi}(a, s'). \quad (44)$$

Since Wasserstein distance is the infimum over all couplings, it follows that:

$$W_p^p((\mathcal{T}^\pi p_\theta^\pi)(\cdot | s), (\mathcal{T}^\pi p_{\theta'}^\pi)(\cdot | s)) \leq \int \int |x - y|^p d\hat{\xi}(x, y). \quad (45)$$

Expanding the right-hand side using the definition of  $\hat{\xi}$ , we get:

$$\begin{aligned} & \int \int |x - y|^p d\hat{\xi}(x, y) \\ &= \int_{(a, s')} \left( \int \int |x - y|^p d\xi_{a, s'}^*(x, y) \right) dP_{s, \pi}(a, s') \\ &= \int_{(a, s')} W_p^p(\mu_{s, a, s'}^{(\theta)}, \mu_{s, a, s'}^{(\theta')}) dP_{s, \pi}(a, s'), \end{aligned} \quad (46)$$

where the second equality follows from (43) since  $\xi_{a, s'}^*$  is the optimal coupling. Combining (45) and (46), we arrive at:

$$\begin{aligned} & W_p^p((\mathcal{T}^\pi p_\theta^\pi)(\cdot | s), (\mathcal{T}^\pi p_{\theta'}^\pi)(\cdot | s)) \\ & \leq \int_{(a, s')} W_p^p(\mu_{s, a, s'}^{(\theta)}, \mu_{s, a, s'}^{(\theta')}) dP_{s, \pi}(a, s'). \end{aligned} \quad (47)$$

Note that  $\mu_{s, a, s'}^{(\theta)}$  and  $\mu_{s, a, s'}^{(\theta')}$  are obtained via the affine transformation  $z \mapsto r(s, a) + \gamma z$ . By Lemma 2 and Lemma 1, we obtain:

$$W_p^p(\mu_{s, a, s'}^{(\theta)}, \mu_{s, a, s'}^{(\theta')}) = \gamma^p W_p^p(p_\theta^\pi(\cdot | s'), p_{\theta'}^\pi(\cdot | s')). \quad (48)$$

Substituting (48) into (47), we find:

$$\begin{aligned} & W_p^p((\mathcal{T}^\pi p_\theta^\pi)(\cdot | s), (\mathcal{T}^\pi p_{\theta'}^\pi)(\cdot | s)) \\ & \leq \int_{(a, s')} W_p^p(\mu_{s, a, s'}^{(\theta)}, \mu_{s, a, s'}^{(\theta')}) dP_{s, \pi}(a, s') \\ &= \gamma^p \int_{(a, s')} W_p^p(p_\theta^\pi(\cdot | s'), p_{\theta'}^\pi(\cdot | s')) dP_{s, \pi}(a, s') \\ & \leq \gamma^p \bar{W}_p^p(p_\theta^\pi, p_{\theta'}^\pi), \end{aligned} \quad (49)$$

where the last inequality follows from  $W_p^p(p_\theta^\pi(\cdot|s'), p_{\theta'}^\pi(\cdot|s')) \leq \bar{W}_p^p(p_\theta^\pi, p_{\theta'}^\pi)$  and  $\int_{(a,s')} dP_{s,\pi}(a, s') = 1$ .

Taking the  $1/p$ -th power of (49), we deduce:

$$W_p((\mathcal{T}^\pi p_\theta^\pi)(\cdot|s), (\mathcal{T}^\pi p_{\theta'}^\pi)(\cdot|s)) \leq \gamma \bar{W}_p(p_\theta^\pi, p_{\theta'}^\pi). \quad (50)$$

Since (50) holds for all  $s \in \mathcal{S}$ , taking the supremum over  $s$ :

$$\begin{aligned} \bar{W}_p(\mathcal{T}^\pi p_\theta^\pi, \mathcal{T}^\pi p_{\theta'}^\pi) &= \sup_{s \in \mathcal{S}} W_p((\mathcal{T}^\pi p_\theta^\pi)(\cdot|s), (\mathcal{T}^\pi p_{\theta'}^\pi)(\cdot|s)) \\ &\leq \gamma \bar{W}_p(p_\theta^\pi, p_{\theta'}^\pi). \end{aligned} \quad (51)$$

Equation (51) establishes that  $\mathcal{T}^\pi$  is a contraction mapping. By Banach's fixed point theorem, there exists a unique fixed point  $p^\pi$  satisfying  $\mathcal{T}^\pi p^\pi = p^\pi$ . Let  $d_t = \bar{W}_p(p_{\theta_t}^\pi, p^\pi)$  denote the distance between the  $t$ -th iterate and the true value distribution. From Lemma 3, we have:

$$\begin{aligned} d_{t+1} &= \bar{W}_p(p_{\theta_{t+1}}^\pi, p^\pi) \\ &\leq \bar{W}_p(p_{\theta_{t+1}}^\pi, \mathcal{T}^\pi p_{\theta_t}^\pi) + \bar{W}_p(\mathcal{T}^\pi p_{\theta_t}^\pi, p^\pi). \end{aligned} \quad (52)$$

The first term is equal to  $\bar{W}_p(p_{\theta_{t+1}}^\pi, \mathcal{T}^\pi p_{\theta_t}^\pi) = \varepsilon_{t+1}$  by definition. For the second term, using the fixed point property  $p^\pi = \mathcal{T}^\pi p^\pi$  and (51), we obtain:

$$\begin{aligned} \bar{W}_p(\mathcal{T}^\pi p_{\theta_t}^\pi, p^\pi) &= \bar{W}_p(\mathcal{T}^\pi p_{\theta_t}^\pi, \mathcal{T}^\pi p^\pi) \\ &\leq \gamma \bar{W}_p(p_{\theta_t}^\pi, p^\pi) = \gamma d_t. \end{aligned} \quad (53)$$

Combining (52) and (53), we conclude:

$$d_{t+1} \leq \varepsilon_{t+1} + \gamma d_t. \quad (54)$$

Since  $\varepsilon_{t+1} \leq \varepsilon_{\max}$  for all  $t \geq 0$  by assumption, it follows that:

$$d_{t+1} \leq \varepsilon_{\max} + \gamma d_t. \quad (55)$$

Iterating (55), we derive:

$$\begin{aligned} d_t &\leq \varepsilon_{\max} + \gamma d_{t-1} \\ &\leq \varepsilon_{\max} + \gamma(\varepsilon_{\max} + \gamma d_{t-2}) \\ &= \varepsilon_{\max} \sum_{j=0}^{t-1} \gamma^j + \gamma^t d_0. \end{aligned} \quad (56)$$

Taking the limit superior as  $t \rightarrow \infty$  in (56), we get:

$$\limsup_{t \rightarrow \infty} d_t \leq \varepsilon_{\max} \cdot \frac{1}{1 - \gamma} + 0 = \frac{\varepsilon_{\max}}{1 - \gamma}, \quad (57)$$

where we use  $\gamma^t d_0 \rightarrow 0$  as  $t \rightarrow \infty$  since  $\gamma \in [0, 1)$ .

Therefore, we establish:

$$\limsup_{t \rightarrow \infty} \bar{W}_p(p_{\theta_t}^\pi, p^\pi) \leq \frac{\varepsilon_{\max}}{1 - \gamma}. \quad (58)$$

Hence the proof is complete.  $\square$

**Corollary 1.** *The velocity field clipping mechanism in Eq. (22) with threshold  $\delta$  ensures the bounded error condition  $\varepsilon_{k+1} \leq \varepsilon_{\max}$  required by Theorem 1.*

*Proof.* The clipping mechanism regularizes gradients during optimization. This directly bounds the parameter update magnitude, and we have:

$$\|\theta_{k+1} - \theta_k\| \leq C_1(\delta), \quad (59)$$

where  $C_1(\delta)$  is a constant determined by the clipping threshold  $\delta$  and the learning rate. By Lipschitz continuity

of the velocity field  $f_\theta$  with respect to  $\theta$ , and the continuous dependence of ODE solutions on parameters, we obtain:

$$\bar{W}_p(p_{\theta_{k+1}}^\pi, p_{\theta_k}^\pi) \leq C_2(\delta), \quad (60)$$

By Lemma 3, we derive:

$$\begin{aligned} \varepsilon_{k+1} &= \bar{W}_p(p_{\theta_{k+1}}^\pi, \mathcal{T}^\pi p_{\theta_k}^\pi) \\ &\leq \bar{W}_p(p_{\theta_{k+1}}^\pi, p_{\theta_k}^\pi) + \bar{W}_p(p_{\theta_k}^\pi, \mathcal{T}^\pi p_{\theta_k}^\pi) \\ &\leq C_2(\delta) + \varepsilon_k. \end{aligned} \quad (61)$$

Iterating inequality (61), we obtain:

$$\varepsilon_n \leq n \cdot C_2(\delta) + \varepsilon_0. \quad (62)$$

Hence the proof is complete.  $\square$

**Theorem 2** (Variance Reduction via CoV Weighting). *Consider the CoV-weighted policy gradient estimator of FlowCritic:*

$$\hat{g}_w = \frac{1}{N_e \cdot T} \sum_{k=1}^{N_e} \sum_{t=0}^{T-1} w_t^{(k)} \cdot \nabla_\theta \log \pi_\theta(a_t^{(k)} | s_t^{(k)}) \cdot \hat{A}_t^{(k)}.$$

The sampling follows Section 3.3, with  $N_e$  parallel environments each generating trajectories of length  $T$ . Then there exists  $\alpha > 0$  such that:

$$\text{Var}[\hat{g}_w] < \text{Var}[\hat{g}],$$

where  $\hat{g}$  denotes the unweighted policy gradient estimator.

*Proof.* Let  $g_t^{(k)} = \nabla_\theta \log \pi_\theta(a_t^{(k)} | s_t^{(k)}) \cdot \hat{A}_t^{(k)}$ . Assuming sample independence, the variance of the unweighted estimator  $\hat{g} = \frac{1}{N_e \cdot T} \sum_{k=1}^{N_e} \sum_{t=0}^{T-1} g_t^{(k)}$  is

$$\text{Var}[\hat{g}] = \frac{1}{(N_e \cdot T)^2} \sum_{k=1}^{N_e} \sum_{t=0}^{T-1} \|\nabla_\theta \log \pi_\theta(a_t^{(k)} | s_t^{(k)})\|^2 \cdot \text{Var}[\hat{A}_t^{(k)}]. \quad (63)$$

Since the value estimate  $\hat{V}(s_t^{(k)}) = \frac{1}{n} \sum_{i=1}^n z_{t,i}^{(k)}$  is computed from  $n$  samples, we have:

$$\text{Var}[\hat{V}(s_t^{(k)})] = \text{Var} \left[ \frac{1}{n} \sum_{i=1}^n z_{t,i}^{(k)} \right] = \frac{(\sigma_t^{(k)})^2}{n}, \quad (64)$$

where  $(\sigma_t^{(k)})^2$  is the variance of the return distribution at state  $s_t^{(k)}$ . From the definition in (30), we obtain:

$$(\sigma_t^{(k)})^2 = (\kappa_t^{(k)})^2 \cdot (|\mu_t^{(k)}| + \varepsilon)^2. \quad (65)$$

Substituting (65) yields into (64) yields, we get:

$$\text{Var}[\hat{V}(s_t^{(k)})] = \frac{(\kappa_t^{(k)})^2 \cdot (|\mu_t^{(k)}| + \varepsilon)^2}{n}. \quad (66)$$

According to the GAE formulation, the variance of the advantage estimate can be expressed as:

$$\text{Var}[\hat{A}_t^{(k)}] \approx \sum_{l=0}^{T-t-1} (\gamma \lambda)^{2l} \cdot \frac{(\kappa_{t+l}^{(k)})^2 \cdot (|\mu_{t+l}^{(k)}| + \varepsilon)^2}{n}. \quad (67)$$

This leads to the following relationship:

$$\text{Var}[\hat{A}_t^{(k)}] \propto (\kappa_t^{(k)})^2. \quad (68)$$

Based on (68), without loss of generality, we set  $\text{Var}[\hat{A}_t^{(k)}] = (\kappa_t^{(k)})^2$  and  $\|\nabla_\theta \log \pi_\theta(a_t^{(k)} | s_t^{(k)})\|^2 = 1$ . To simplify notation, we define the total sample size  $N = N_e \cdot T$

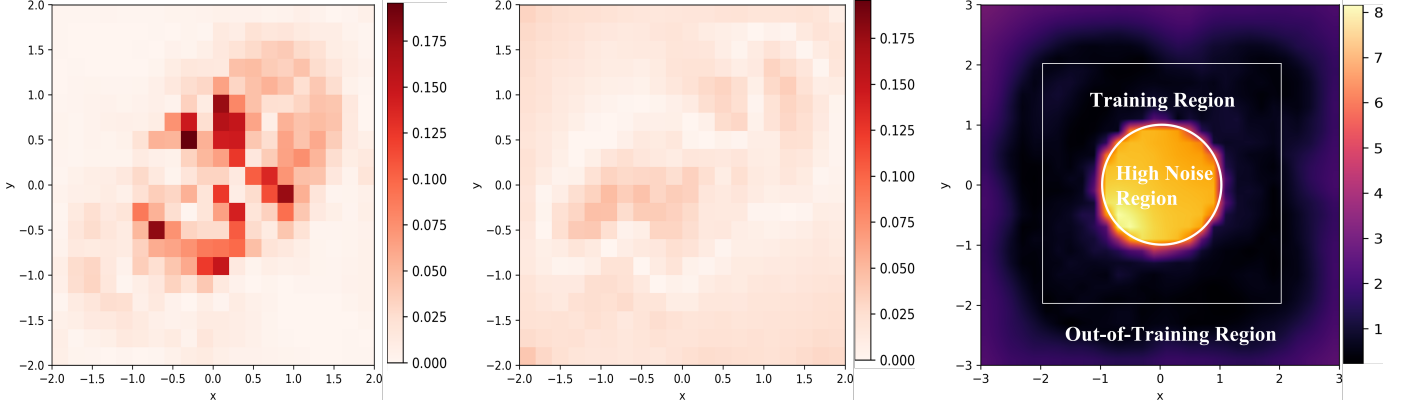


Fig. 2. Results on the single-step environment.

and replace the double summation with a single index  $i \in \{1, \dots, N\}$ , where  $\kappa_i$  corresponds to  $\kappa_t^{(k)}$ . The variances of the unweighted and weighted gradient estimators are given by:

$$\text{Var}[\hat{g}] = \frac{1}{N^2} \sum_{i=1}^N \kappa_i^2, \quad (69)$$

$$\text{Var}[\hat{g}_w] = \frac{1}{N^2} \sum_{i=1}^N \hat{w}_i^2 \kappa_i^2 = \frac{\sum_{i=1}^N e^{-2\alpha\kappa_i} \kappa_i^2}{(\sum_{j=1}^N e^{-\alpha\kappa_j})^2}. \quad (70)$$

Then, we define the auxiliary function  $\phi(\alpha) = \text{Var}[\hat{g}_w] - \text{Var}[\hat{g}]$ . Clearly,  $\phi(0) = 0$  since both estimators are identical when  $\alpha = 0$ . Computing the derivative at  $\alpha = 0$ , we have:

$$\begin{aligned} \phi'(0) &= \frac{d}{d\alpha} \left[ \frac{\sum_i e^{-2\alpha\kappa_i} \kappa_i^2}{(\sum_j e^{-\alpha\kappa_j})^2} \right]_{\alpha=0} \\ &= \frac{2}{N^3} \left( \sum_{i=1}^N \kappa_i^2 \sum_{j=1}^N \kappa_j - N \sum_{i=1}^N \kappa_i^3 \right). \end{aligned} \quad (71)$$

By the Chebyshev sum inequality, when  $\{\kappa_i\}$  are not all equal, we derive

$$\sum_{i=1}^N \kappa_i^2 \sum_{j=1}^N \kappa_j < N \sum_{i=1}^N \kappa_i^3. \quad (72)$$

Therefore  $\phi'(0) < 0$ . Since  $\phi(0) = 0$  and  $\phi'(0) < 0$ , there exists  $\alpha > 0$  such that  $\phi(\alpha) < 0$ , which implies  $\text{Var}[\hat{g}_w] < \text{Var}[\hat{g}]$ . Hence the proof is complete.  $\square$

## 5 EXPERIMENTS

To comprehensively evaluate the effectiveness of our proposed FlowCritic algorithm, we conduct a series of comparative experiments and ablation studies across diverse environments. These experiments are designed to answer the following questions: (1) In stochastic environments, what advantages does FlowCritic's modeling of the complete state-value distribution offer over PPO's point estimation method? (2) On complex robotic control tasks, does FlowCritic outperform various baseline methods? (3) How do the different parameters of FlowCritic affect its final performance? (4) Can policies trained by FlowCritic be effectively deployed on real-world physical systems?

TABLE 1. Hyperparameter settings for the control tasks.

Parameter	Value
<i>Shared Parameters (PPO, PPO_AVC, PPO_CVE, PPO_QD &amp; FlowCritic)</i>	
Number of parallel environments ( $N_e$ )	1024
Rollout length ( $T$ )	16
Epochs per iteration ( $K$ )	4
Optimizer	Adam
Learning Rate	5e-4
Discount Factor ( $\gamma$ )	0.99
GAE Parameter ( $\lambda$ )	0.95
PPO Clip Ratio ( $\epsilon$ )	0.2
Minibatches	2
Minibatch Size	8192
Advantage Normalization	True
Actor Network Architecture	$[256] \times 2$
Critic Network Architecture	$[512] \times 4$
Actor Activation Function	Tanh
Critic Activation Function	ReLU
Actor-Critic grad norm	1.0
<i>PPO_AVC-Specific Parameters</i>	
Number of critic networks	5
<i>PPO_CVE-Specific Parameters</i>	
Number of critic networks	5
<i>PPO_QD-Specific Parameters</i>	
Number of quantiles	51
Huber loss parameter ( $\kappa$ )	1.0
<i>FlowCritic-Specific Parameters</i>	
Number of generated value estimates ( $n$ )	10
Truncated sample size ( $m$ )	1
Velocity field clipping threshold ( $\delta$ )	0.2
CoV temperature ( $\alpha$ )	0.1

### 5.1 Value Estimation in a Single-Step Environment

In this experiment, following the setup in TQC [30], we construct a single-step decision process to evaluate the performance of point estimation and FlowCritic's flow matching approach in value estimation. The environment is formalized as  $\mathcal{M} = (\mathcal{S}, \mathcal{A}, \rho, R, \gamma)$ , where the state space is defined as  $\mathcal{S} = [-3, 3]^2$ , and states  $s = (x, y)$  are sampled from a uniform distribution  $\rho$ . The action space is given by  $\mathcal{A} = \{a_0\}$ , and each episode terminates after a single step, with the reward depending solely on the current state. The

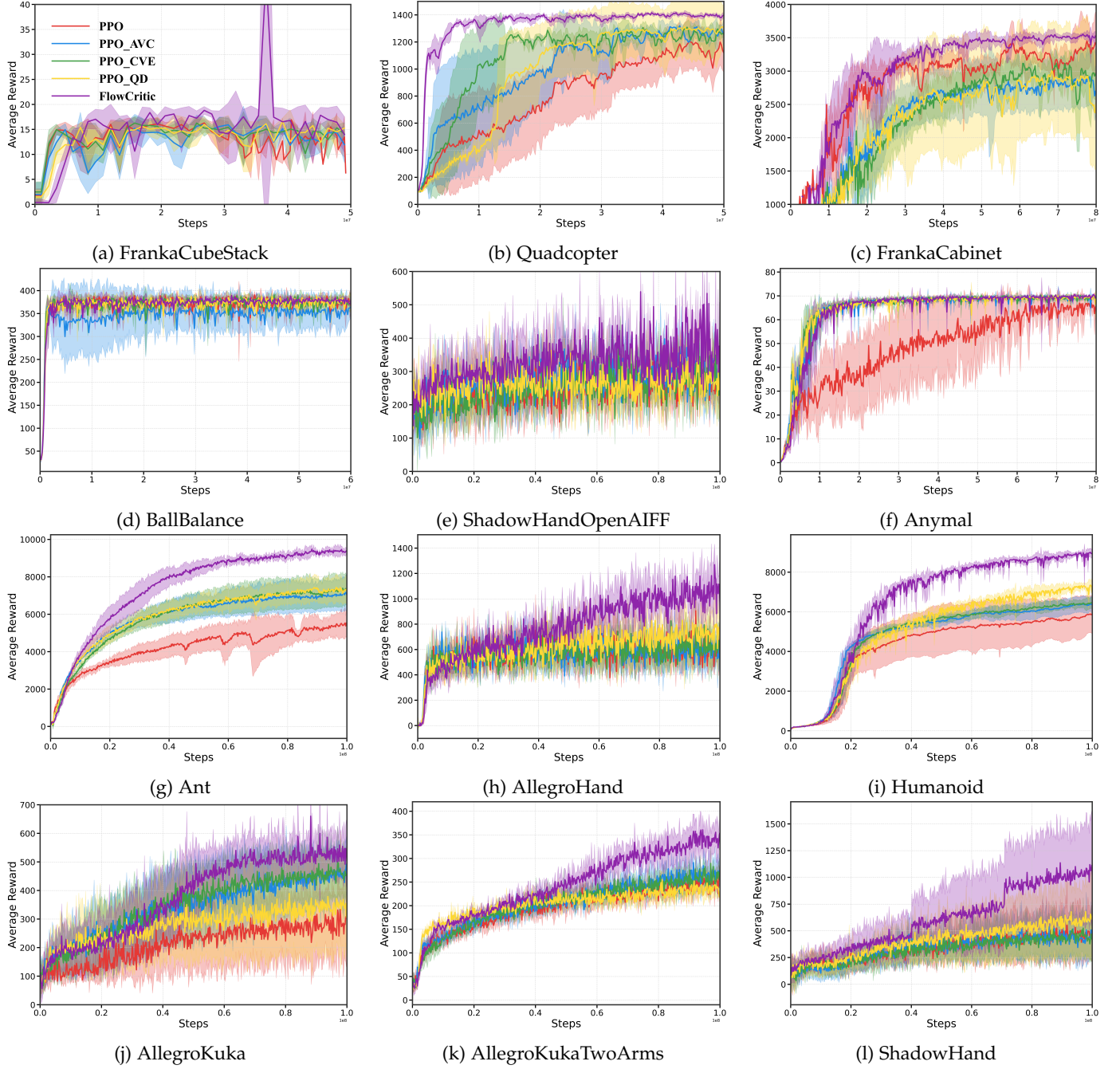


Fig. 3. Learning curves comparisons of FlowCritic (purple), PPO (red), PPO\_AVC (blue), PPO\_CVE (green), and PPO\_QD (yellow) on 12 control benchmark tasks. Solid lines represent mean episodic returns over 5 random seeds, with shaded areas indicating one standard deviation.

true expected value function of  $\mathcal{M}$  is defined as:

$$V^*(x, y) = 1.5 \exp\left(-\frac{\|s - \mu_1\|^2}{2\ell_1^2}\right) - 1.5 \exp\left(-\frac{\|s - \mu_2\|^2}{2\ell_2^2}\right), \quad (73)$$

where  $\mu_1 = (0.8, 0.8)$ ,  $\mu_2 = (-0.8, -0.8)$ , and  $\ell_1 = \ell_2 = 0.5$ . To introduce stochasticity into the environment, the observed reward is defined as:

$$\tilde{R}(s) \sim \begin{cases} (1 - \varepsilon) \mathcal{N}(V^*(s), \sigma_1^2) + \varepsilon \mathcal{N}(V^*(s), \sigma_2^2), & \|s\| \leq 1, \\ \mathcal{N}(V^*(s), \sigma_3^2), & \text{otherwise,} \end{cases} \quad (74)$$

where  $\|s\| = \sqrt{x^2 + y^2}$ . The region  $\|s\| \leq 1$  represents high stochasticity with  $\varepsilon = 0.2$ ,  $\sigma_1 = 0.05$ ,  $\sigma_2 = 10$ ,

and  $\sigma_3 = 0.01$ . We compare the value estimation capabilities of FlowCritic and point estimation methods within the constructed environment. To ensure a fair comparison, both methods adopt an identical neural network architecture, and are trained using data sampled from  $\mathcal{S} = [-2, 2]^2$ . Fig. 2a and Fig. 2b present the absolute errors for point estimation and FlowCritic, respectively. In the high-stochasticity region  $\|s\| \leq 1$ , point estimation suffers from large errors that exceed 0.15 due to outlier noise, while FlowCritic maintains robust predictions with substantially lower errors throughout the state space, attributed to the advantages of flow matching's multiple sampling and value truncation mechanisms.

TABLE 2. Dimensions of control tasks

Environment	Obs. Dimension	Action Dimension
FrankaCubeStack	19	7
Quadcopter	21	12
FrankaCabinet	23	9
BallBalance	24	3
ShadowHandOpenAIFF	42	20
Anymal	48	12
Ant	60	8
AllegroHand	88	16
Humanoid	108	21
AllegroKuka	117	23
AllegroKukaTwoArms	196	46
ShadowHand	211	20

To further analyze the distributional properties captured by FlowCritic, we compute and visualize its CoV across the state space as shown in Fig. 2c using Eq. (30). The CoV heatmap reveals two important characteristics. First, high CoV regions closely match the high noise region  $\|s\| \leq 1$  within the training region  $S = [-2, 2]^2$ , confirming that CoV effectively measures noise levels across samples. This alignment justifies the weighting mechanism in Eq. (31) for suppressing high-noise samples. Second, we observe that the CoV also increases significantly in the out-of-training regions (outside  $S = [-2, 2]^2$ ), where insufficient training data leads to increased noise in the generated value estimates. This further validates the rationality of the weighting strategy in Eq. (31), which can adaptively suppress both high-noise samples.

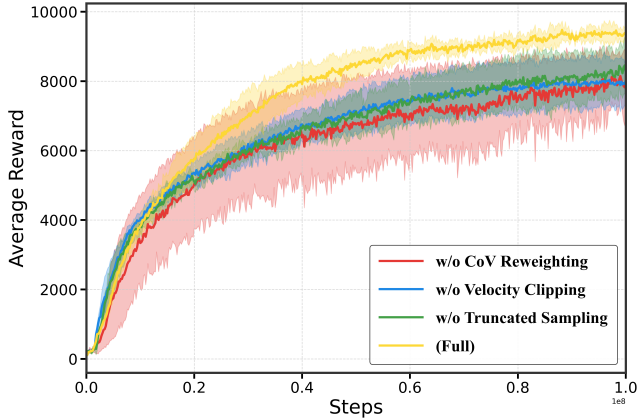


Fig. 4. Ablation study on key components of FlowCritic.

## 5.2 Experimental Setup for Continuous Control Tasks

We evaluate FlowCritic across 12 control tasks spanning a wide range of complexity and dimensionality. As detailed in Table 2, our benchmark environments encompass diverse challenges including complex locomotion, dexterous manipulation, and robotic arm control [40], with observation dimensions ranging from 19 to 211 and action dimensions from 3 to 46. All experiments utilize NVIDIA Isaac Gym, which provides GPU-accelerated parallel simulation [41]. Since FlowCritic extends the on-policy policy gradient paradigm and Isaac Gym’s synchronous, high-throughput data collection is inherently optimized for on-policy algorithms, we focus our evaluation on on-policy

baselines rather than off-policy methods such as SAC or TD3 [19], [42].

To achieve comprehensive performance evaluation, we adapt multiple representative value estimation enhancement techniques to the PPO framework, which has not been undertaken in existing literature. Specifically, we additionally implement the following methods: PPO with Averaged Value Critics (PPO\_AVC), which averages multiple independent critics to reduce estimation variance [20], [23]; PPO with Conservative Value Ensemble (PPO\_CVE), which adopts the conservative strategy from SAC-N to enhance the robustness of value estimation [22]; and PPO with Quantile Distribution (PPO\_QD), which integrates the quantile modeling principles from QR-DQN and TQC to learn complete value distributions through quantile regression [26], [30].

To ensure fair comparisons, all algorithms adopt identical network architectures and share a common set of core hyperparameters (detailed in Table 1). Algorithm performance is measured by average episodic return. For statistical robustness, all results are aggregated over five independent runs with different random seeds. In tabular results, we report performance over the final 10% of training. In learning curves, we present mean return evaluated every 200,000 steps, with shaded regions representing one standard deviation.

## 5.3 Performance Comparisons

Figure 3 and Table 3 present the learning curves and final performance comparisons across 12 control benchmark environments. Among the baseline methods, PPO\_AVC, PPO\_CVE, and PPO\_QD outperform standard PPO in most tasks. However, these methods exhibit inconsistent performance across tasks, with certain variants even underperforming standard PPO in specific environments, thereby revealing inherent limitations in their value estimation approaches. In contrast, FlowCritic consistently surpasses all baseline methods across all 12 environments, often by substantial margins. This performance advantage becomes particularly pronounced in high-dimensional complex manipulation tasks such as Ant, AllegroHand, and ShadowHand, while even in lower-dimensional environments, FlowCritic exhibits reduced standard deviation, demonstrating superior training stability. The experimental results demonstrate the superior performance of FlowCritic over existing algorithms through modeling value distributions via flow matching and adaptively exploiting distributional information.

## 5.4 Ablation Studies

To gain deeper insights into the contribution of each FlowCritic component to the final performance, we conduct systematic ablation studies on the Ant environment. We select Ant because it exhibits moderate complexity and favorable training stability, enabling clear observation of individual component effects while other environments demonstrate similar trends.

### 5.4.1 Core Component Ablation

We sequentially remove key components of FlowCritic to assess their impact on performance, with results presented

TABLE 3. Final performance comparisons between FlowCritic and baselines.

Environment	PPO	PPO_AVG	PPO_CVE	PPO_QD	FlowCritic (Ours)
FrankaCubeStack	$11.93 \pm 2.69$	$13.29 \pm 1.22$	$14.20 \pm 1.19$	$14.36 \pm 1.09$	<b><math>16.30 \pm 1.63</math></b>
Quadcopter	$1131.08 \pm 156.59$	$1271.63 \pm 48.38$	$1244.01 \pm 39.94$	$1289.69 \pm 218.54$	<b><math>1393.56 \pm 6.95</math></b>
FrankaCabinet	$3291.96 \pm 354.19$	$2822.75 \pm 372.00$	$2873.50 \pm 326.68$	$2776.54 \pm 797.23$	<b><math>3511.01 \pm 33.21</math></b>
BallBalance	$373.88 \pm 2.55$	$354.01 \pm 33.83$	$374.25 \pm 2.33$	$374.41 \pm 3.89$	<b><math>377.87 \pm 1.38</math></b>
ShadowHandOpenAIFF	$269.38 \pm 14.77$	$283.04 \pm 23.60$	$282.93 \pm 18.10$	$272.69 \pm 15.78$	<b><math>376.99 \pm 30.59</math></b>
Anymal	$65.03 \pm 4.45$	$69.13 \pm 0.54$	$69.13 \pm 0.21$	$69.22 \pm 0.43$	<b><math>69.63 \pm 0.16</math></b>
Ant	$5340.04 \pm 614.56$	$7009.38 \pm 835.03$	$7224.92 \pm 832.91$	$7269.09 \pm 642.77$	<b><math>9345.29 \pm 182.16</math></b>
AllegroHand	$604.59 \pm 16.04$	$594.16 \pm 33.88$	$630.61 \pm 48.91$	$721.03 \pm 142.61$	<b><math>1044.12 \pm 103.53</math></b>
Humanoid	$5713.11 \pm 1043.47$	$6330.85 \pm 394.06$	$6385.10 \pm 210.36$	$7196.31 \pm 194.23$	<b><math>8863.61 \pm 114.08</math></b>
AllegroKuka	$281.86 \pm 114.90$	$451.39 \pm 87.52$	$460.17 \pm 84.89$	$344.34 \pm 154.83$	<b><math>529.30 \pm 50.44</math></b>
AllegroKukaTwoArms	$248.88 \pm 6.75$	$264.88 \pm 21.73$	$259.26 \pm 6.77$	$235.83 \pm 12.80$	<b><math>339.87 \pm 27.00</math></b>
ShadowHand	$465.08 \pm 237.48$	$435.71 \pm 175.31$	$444.01 \pm 165.05$	$594.72 \pm 329.38$	<b><math>1025.76 \pm 427.69</math></b>

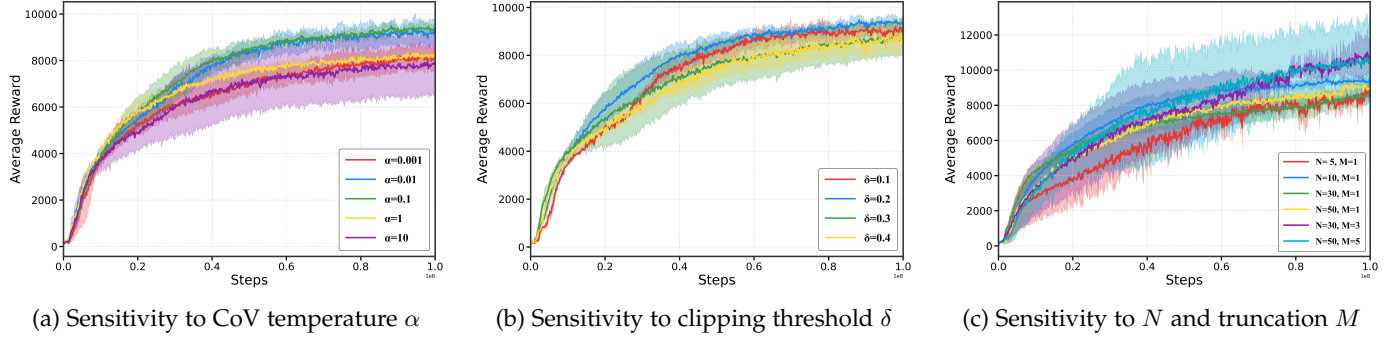


Fig. 5. Sensitivity analysis of key hyperparameters of FlowCritic.



(a) Omnidirectional locomotion in cluttered environment



(b) Stair climbing on stepped platforms

Fig. 6. Real-world deployment on Unitree Go2 quadrupedal robot.

in Fig. 4. Removing CoV reweighting causes the most substantial performance drop throughout training, validating its critical role in improving sample efficiency. In contrast, removing velocity clipping or truncated sampling maintains comparable early-stage performance but exhibits progressively increased variance (wider shaded regions), highlighting their importance for long-term training stability.

**5.4.2 Hyperparameter Sensitivity and Component Synergy**  
Building upon the validation of component effectiveness, we conduct sensitivity analysis of key hyperparameters, with results presented in Fig. 5. Fig. 5a illustrates the

impact of CoV temperature parameter  $\alpha$ , which controls the concentration of weight. Smaller values strongly suppress the weights of high-noise samples, while larger values yield nearly uniform weighting. The results show that  $\alpha = 0.1$  and  $\alpha = 0.01$  exhibit similar learning curves throughout training and achieve optimal performance. Figure 5b demonstrates the sensitivity to velocity field clipping threshold  $\delta$ . Smaller thresholds impose stronger constraints on gradient updates, while larger thresholds relax these restrictions. The experiments show that  $\delta = 0.2$  and  $\delta = 0.1$  achieve comparable final performance. Based on these observations, we set  $\alpha = 0.1$  and  $\delta = 0.2$  as default

hyperparameters throughout this work.

Furthermore, Fig. 5c reveals significant synergistic effects between the number of sampled value estimates  $N$  and truncation size  $M$ . We evaluate combinations of  $N \in \{5, 10, 30, 50\}$  and  $M \in \{1, 3, 5\}$ . The results show that naively increasing  $N$  alone does not monotonically improve performance, as  $N = 50, M = 1$  even underperforms  $N = 10, M = 1$ , since larger sample size  $N$  may introduce additional outlier estimates that degrade learning quality without proper truncation. In contrast, jointly scaling both  $N$  and  $M$  yields substantial performance gains, with  $N = 30, M = 3$  achieving notably superior returns while further increasing to  $N = 50, M = 5$  provides only limited marginal improvement. This demonstrates that effective synergy requires pairing larger sample size with proportional truncation to filter noise. Balancing computational cost against performance, we adopt  $N = 10, M = 1$  as the default configuration throughout our experiments.

## 5.5 Real Quadrupedal Robot Deployment

We deploy trained FlowCritic policies on the Unitree Go2 quadrupedal robot to validate their practical effectiveness. Policies trained in Isaac Gym transfer directly to hardware without sim-to-real adaptation, executing at 50Hz with a 454-dimensional state space that incorporates observations and privileged information, and a 12-dimensional action space for joint control. As shown in Fig. 6, we evaluate FlowCritic in two scenarios. Fig. 6a shows omnidirectional locomotion in cluttered environments with wooden sticks and spherical obstacles, where the robot maintains stable gait and flexible movement. Fig. 6b shows stair climbing on stepped platforms, where the robot adapts to elevation changes while maintaining balance. Both tasks validate effective real-world deployment of FlowCritic.

## 6 CONCLUSION

In this paper, we have introduced the FlowCritic, a novel framework that is the first to apply generative models for value distribution representation in RL. FlowCritic introduces innovations in two key areas: the flexible representation of the value distribution and the effective utilization of its statistical information. It employs a flow matching generative model to accurately capture arbitrarily complex value distributions, overcoming the representation limitations of conventional methods. Concurrently, FlowCritic pioneers an adaptive weighting mechanism based on the CoV that integrates statistical properties of the value distribution beyond its expectation into the policy update process, thereby achieving more robust policy updates. The superiority and practicality of FlowCritic are substantiated by both theoretical analysis and extensive experiments on challenging control benchmarks and a physical quadruped robot, demonstrating performance that significantly surpasses existing baseline algorithms. Future research will explore integrating more efficient generative models to reduce the training overhead of FlowCritic, as well as extending it to multi-agent reinforcement learning, where distributional modeling can better capture inter-agent coordination dynamics. In addition, applying FlowCritic to continual

learning scenarios, where value distributions evolve with changing environments, represents a promising direction for lifelong learning systems.

## REFERENCES

- [1] T. Miki, J. Lee, J. Hwangbo, L. Wellhausen, V. Koltun, and M. Hutter, "Learning robust perceptive locomotion for quadrupedal robots in the wild," *Science robotics*, vol. 7, no. 62, p. eabk2822, 2022.
- [2] J. Hwangbo, J. Lee, A. Dosovitskiy, D. Bellicoso, V. Tsounis, V. Koltun, and M. Hutter, "Learning agile and dynamic motor skills for legged robots," *Science Robotics*, vol. 4, no. 26, p. eaau5872, 2019.
- [3] E. Yousefi, M. Chen, and I. Sharf, "Baseline policy adapting and abstraction of shared autonomy for high-level robot operations," *IEEE Transactions on Robotics*, 2025.
- [4] C. Huang, G. Wang, Z. Zhou, R. Zhang, and L. Lin, "Reward-adaptive reinforcement learning: Dynamic policy gradient optimization for bipedal locomotion," *IEEE Transactions on Pattern Analysis and Machine Intelligence*, vol. 45, no. 6, pp. 7686–7695, 2022.
- [5] Z. Zhu, K. Lin, A. K. Jain, and J. Zhou, "Transfer learning in deep reinforcement learning: A survey," *IEEE Transactions on Pattern Analysis and Machine Intelligence*, 2023.
- [6] R. Zhao, Y. Li, Y. Fan, F. Gao, M. Tsukada, and Z. Gao, "A survey on recent advancements in autonomous driving using deep reinforcement learning: Applications, challenges, and solutions," *IEEE Transactions on Intelligent Transportation Systems*, 2024.
- [7] Q. Li, Z. Peng, L. Feng, Q. Zhang, Z. Xue, and B. Zhou, "Metadrive: Composing diverse driving scenarios for generalizable reinforcement learning," *IEEE Transactions on Pattern Analysis and Machine Intelligence*, vol. 45, no. 3, pp. 3461–3475, 2022.
- [8] L. Ouyang, J. Wu, X. Jiang, D. Almeida, C. Wainwright, P. Mishkin, C. Zhang, S. Agarwal, K. Slama, A. Ray *et al.*, "Training language models to follow instructions with human feedback," *Advances in neural information processing systems*, vol. 35, pp. 27730–27744, 2022.
- [9] D. Guo, D. Yang, H. Zhang, J. Song, P. Wang, Q. Zhu, R. Xu, R. Zhang, S. Ma, X. Bi *et al.*, "Deepseek-r1 incentivizes reasoning in llms through reinforcement learning," *Nature*, vol. 645, no. 8081, pp. 633–638, 2025.
- [10] R. S. Sutton and A. G. Barto, *Reinforcement learning: An introduction*. MIT press, 2018.
- [11] K. Arulkumaran, M. P. Deisenroth, M. Brundage, and A. A. Bharath, "Deep reinforcement learning: A brief survey," *IEEE signal processing magazine*, vol. 34, no. 6, pp. 26–38, 2017.
- [12] R. F. Prudencio, M. R. Maximo, and E. L. Colombini, "A survey on offline reinforcement learning: Taxonomy, review, and open problems," *IEEE Transactions on Neural Networks and Learning Systems*, vol. 35, no. 8, pp. 10237–10257, 2023.
- [13] V. Mnih, K. Kavukcuoglu, D. Silver, A. A. Rusu, J. Veness, M. G. Bellemare, A. Graves, M. Riedmiller, A. K. Fidjeland, G. Ostrovski *et al.*, "Human-level control through deep reinforcement learning," *nature*, vol. 518, no. 7540, pp. 529–533, 2015.
- [14] R. S. Sutton, D. McAllester, S. Singh, and Y. Mansour, "Policy gradient methods for reinforcement learning with function approximation," *Advances in neural information processing systems*, vol. 12, 1999.
- [15] D. Wu, X. Dong, J. Shen, and S. C. Hoi, "Reducing estimation bias via triplet-average deep deterministic policy gradient," *IEEE transactions on neural networks and learning systems*, vol. 31, no. 11, pp. 4933–4945, 2020.
- [16] C. Wu, A. Rajeswaran, Y. Duan, V. Kumar, A. M. Bayen, S. Kakade, I. Mordatch, and P. Abbeel, "Variance reduction for policy gradient with action-dependent factorized baselines," *arXiv preprint arXiv:1803.07246*, 2018.
- [17] J. Schulman, P. Moritz, S. Levine, M. I. Jordan, and P. Abbeel, "High-dimensional continuous control using generalized advantage estimation," in *4th International Conference on Learning Representations, ICLR 2016, San Juan, Puerto Rico, May 2-4, 2016, Conference Track Proceedings*, Y. Bengio and Y. LeCun, Eds., 2016.
- [18] H. Hasselt, "Double q-learning," *Advances in neural information processing systems*, vol. 23, 2010.
- [19] S. Fujimoto, H. Hoof, and D. Meger, "Addressing function approximation error in actor-critic methods," in *International conference on machine learning*. PMLR, 2018, pp. 1587–1596.

[20] O. Anschel, N. Baram, and N. Shimkin, "Averaged-dqn: Variance reduction and stabilization for deep reinforcement learning," in *International conference on machine learning*. PMLR, 2017, pp. 176–185.

[21] Q. Lan, Y. Pan, A. Fyshe, and M. White, "Maxmin q-learning: Controlling the estimation bias of q-learning," *arXiv preprint arXiv:2002.06487*, 2020.

[22] G. An, S. Moon, J.-H. Kim, and H. O. Song, "Uncertainty-based offline reinforcement learning with diversified q-ensemble," *Advances in neural information processing systems*, vol. 34, pp. 7436–7447, 2021.

[23] F. Zargarbashi, J. Cheng, D. Kang, R. Sumner, and S. Coros, "Robotkeyframing: Learning locomotion with high-level objectives via mixture of dense and sparse rewards," *arXiv preprint arXiv:2407.11562*, 2024.

[24] M. G. Bellemare, W. Dabney, and R. Munos, "A distributional perspective on reinforcement learning," in *International Conference on Machine Learning*. PMLR, 2017, pp. 449–458.

[25] M. G. Bellemare, W. Dabney, and M. Rowland, *Distributional reinforcement learning*. MIT Press, 2023.

[26] W. Dabney, M. Rowland, M. Bellemare, and R. Munos, "Distributional reinforcement learning with quantile regression," in *Proceedings of the AAAI conference on artificial intelligence*, vol. 32, no. 1, 2018.

[27] W. Dabney, G. Ostrovski, D. Silver, and R. Munos, "Implicit quantile networks for distributional reinforcement learning," in *International Conference on Machine Learning*. PMLR, 2018, pp. 1096–1105.

[28] J. Duan, Y. Guan, S. E. Li, Y. Ren, Q. Sun, and B. Cheng, "Distributional soft actor-critic: Off-policy reinforcement learning for addressing value estimation errors," *IEEE Transactions on Neural Networks and Learning Systems*, 2022.

[29] J. Duan, W. Wang, L. Xiao, J. Gao, S. E. Li, C. Liu, Y.-Q. Zhang, B. Cheng, and K. Li, "Distributional soft actor-critic with three refinements," *IEEE Transactions on Pattern Analysis and Machine Intelligence*, 2025.

[30] A. Kuznetsov, P. Shvechikov, A. Grishin, and D. Vetrov, "Controlling overestimation bias with truncated mixture of continuous distributional quantile critics," in *International conference on machine learning*. PMLR, 2020, pp. 5556–5566.

[31] J. Farebrother, J. Orbay, Q. Vuong, A. A. Taiga, Y. Chebotar, T. Xiao, A. Irpan, S. Levine, P. S. Castro, A. Faust *et al.*, "Stop regressing: Training value functions via classification for scalable deep rl," in *International Conference on Machine Learning*. PMLR, 2024, pp. 13 049–13 071.

[32] K. Sun, B. Jiang, and L. Kong, "How does return distribution in distributional reinforcement learning help optimization?" in *ICML 2024 Workshop: Aligning Reinforcement Learning Experimentalists and Theorists*.

[33] J. Ho, A. Jain, and P. Abbeel, "Denoising diffusion probabilistic models," *Advances in Neural Information processing Systems*, vol. 33, pp. 6840–6851, 2020.

[34] J. Song, C. Meng, and S. Ermon, "Denoising diffusion implicit models," in *9th International Conference on Learning Representations, ICLR 2021, Virtual Event, Austria, May 3-7, 2021*, 2021.

[35] Y. Lipman, R. T. Q. Chen, H. Ben-Hamu, M. Nickel, and M. Le, "Flow matching for generative modeling," in *The Eleventh International Conference on Learning Representations, ICLR 2023*, 2023.

[36] X. Liu, C. Gong, and Q. Liu, "Flow straight and fast: Learning to generate and transfer data with rectified flow," *arXiv preprint arXiv:2209.03003*, 2022.

[37] R. S. Sutton, A. G. Barto *et al.*, *Reinforcement learning: An introduction*. MIT press Cambridge, 1998, vol. 1, no. 1.

[38] M. S. Albergo and E. Vanden-Eijnden, "Building normalizing flows with stochastic interpolants," *arXiv preprint arXiv:2209.15571*, 2022.

[39] J. Schulman, F. Wolski, P. Dhariwal, A. Radford, and O. Klimov, "Proximal policy optimization algorithms," *arXiv preprint arXiv:1707.06347*, 2017.

[40] E. Todorov, T. Erez, and Y. Tassa, "Mujoco: A physics engine for model-based control," in *2012 IEEE/RSJ international conference on intelligent robots and systems*. IEEE, 2012, pp. 5026–5033.

[41] V. Makoviychuk, L. Wawrzyniak, Y. Guo, M. Lu, K. Storey, M. Macklin, D. Hoeller, N. Rudin, A. Allshire, A. Handa *et al.*, "Isaac gym: High performance gpu-based physics simulation for robot learning," *arXiv preprint arXiv:2108.10470*, 2021.

[42] T. Haarnoja, A. Zhou, P. Abbeel, and S. Levine, "Soft actor-critic: Off-policy maximum entropy deep reinforcement learning with a stochastic actor," in *Proceedings of the 35th International Conference on Machine Learning, ICML 2018*, vol. 80. PMLR, 2018, pp. 1856–1865.